Published in final edited form as:
Biomaterials. 2014 September ; 35(28): 8134–8143. doi:10.1016/j.biomaterials.2014.06.009.

Temporal and spatial patterning of transgene expression by near-infrared irradiation

Francisco M. Martin-Saavedra[#a,b], **Virginia Cebrian**[#b,a], **Leyre Gomez**[c], **Daniel Lopez**[d], **Manuel Arruebo**[c,a], **Christopher G Wilson**[e], **Renny T. Franceschi**[e], **Richard Voellmy**[f,g], **Jesus Santamaria**[c,a], and **Nuria Vilaboa**[b,a,*]

[a]CIBER de Bioingeniería, Biomateriales y Nanomedicina (CIBER-BBN), 28029 Madrid, Spain [b]Hospital Universitario La Paz-IdiPAZ, 28046 Madrid, Spain [c]Department of Chemical Engineering, Nanoscience Institute of Aragon (INA), University of Zaragoza, 50018 Zaragoza, Spain [d]Institute of Polymer Science and Technology (ICTP-CSIC), 28006 Madrid, Spain [e]Center for Craniofacial Regeneration and Department of Periodontics and Oral Medicine, University of Michigan School of Dentistry, Ann Arbor, MI 48109, USA [f]Department of Physiological Sciences, University of Florida, Gainesville, FL 32611, USA [g]HSF Pharmaceuticals S.A., 1814 La Tour-de-Peilz, Switzerland

[#] These authors contributed equally to this work.

Abstract

We investigated whether near-infrared (NIR) light could be employed for patterning transgene expression in plasmonic cell constructs. Hollow gold nanoparticles with a plasmon surface band absorption peaking at ~750 nm, a wavelength within the so called “tissue optical window”, were used as fillers in fibrin-based hydrogels. These composites, which efficiently transduce NIR photon energy into heat, were loaded with genetically-modified cells that harbor a heat-activated and ligand-dependent gene switch for regulating transgene expression. NIR laser irradiation in the presence of ligand triggered 3-dimensional patterns of transgene expression faithfully matching the illuminated areas of plasmonic cell constructs. This noninvasive technology was proven useful for remotely controlling *in vivo* the spatiotemporal bioavailability of transgenic vascular endothelial growth factor. The combination of spatial control by means of NIR irradiation along with safe and timed transgene induction presents a high application potential for engineering tissues in regenerative medicine scenarios.

[*]Corresponding author. Tel.: +34 912071034; fax: +34 917277524. nuria.vilaboa@salud.madrid.org..

1. Introduction

Engineered functional tissues must achieve a high level of cellular organization in structures that resemble those intended to be replaced. To accomplish this, major research efforts have been undertaken to develop scaffolds that mimic the geometry of the replaced tissue and provide a 3-dimensional environment that supports specific cell function. A multitude of signaling factors, many of which have well established roles in tissue development and homeostasis, regulates interactions and behavior of cells seeded in scaffolds. However, recapitulating the production of control factors responsible for native tissue formation over appropriate spatial and time scales remains a central challenge in regenerative medicine.

Scaffolds may instruct surrounding environments by releasing bioactive agents. Most porous scaffolds currently used in tissue engineering deliver cargos passively, through mechanisms of molecular diffusive transport that provide limited control on release kinetics and hamper the effectiveness of the approach. Recently, the implementation of nanotechnology-enabled strategies in the design of porous scaffolds has made possible triggered delivery of growth factors and signaling molecules using external stimuli. Examples of these strategies are porous ferrogels intended to control locally the cellular microenvironment through the release of recombinant regenerative factors such as SDF1-α [1] or FGF-2 [2] subsequent to magnetic stimulation. Such approaches usually involve a burst release of therapeutic agent after stimulus application that precludes the re-induction of the system and limits its long-term functionality.

Alternatively, precise control over the production and the subsequent release of growth factors and signaling molecules from scaffolds can be achieved by seeding these substrates with cells that are genetically engineered to express the latter bioactive factors. In this case, external activation is also a desirable feature to achieve control over the release profile of targeted factors. In this regard, gene therapy systems that employ promoters sensitive to physical stimuli such as light, ionizing radiation or heat [3,4] are promising tools for remotely controlling the spatiotemporal bioavailability of therapeutic proteins. The promoter of the *HSP70B* gene (*HSPA7*), one of the most highly heat-inducible genes [5], has been successfully used for local control of transgene expression in combination with noninvasive methods for focused heating such as ultrasound [6,7]. A key to realizing the full potential of this approach is the development of reliable, non-invasive methods capable of heating deep-seated areas without causing tissue harm. It is noted that excessive acoustic pressure and high temperature from focused ultrasound may generate cavitation leading to tissue damage [6,8].

Plasmonic photothermia, in which photon energy is converted into heat by photothermal nanotransducers, is a nanotechnology resource that can be adapted for inducing *HSP*-based gene expression systems [9,10]. On account of the phenomenon of localized surface plasmon resonance (LSPR), gold nanoparticles (GNPs) exhibit strong visible and near-infrared light absorption that depends on the size, shape and surrounding medium of the nanomaterial. The ability to control GNP dimensions makes it possible to prepare nanostructures tailored for absorption between 650 and 950 nm. This wavelength range that

does not include the major absorption peaks of blood and water provides a therapeutic window that maximizes light penetrance in biological tissues [11,12].

In this study, we explore the feasibility of providing plasmonic properties to fibrin hydrogels by the incorporation of hollow gold nanoparticles (HGNPs) [10] and the suitability of the resulting scaffolds to encapsulate cells harboring a transgene expression system triggered by heat and dependent on a dimerizer-controlled chimeric transactivator [13]. We tested whether the combination of NIR irradiation and dimerizer administration induces transgene expression in plasmonic cell constructs implanted in mice, with spatial patterns that match the NIR-illuminated region.

2. Materials and methods

2.1. Vector construction

Coding sequence of enhanced green fluorescent protein (EGFP) was PCR-amplified from pEGFP-C1 (Clontech, Mountain View, CA, USA) using primers 5′-TAGCGCTACTAGTCGCCAC and 5′-GGCTGATATCGATCAGTTATC, digested with SpeI and ClaI and ligated to SpeI/ClaI-cut pZ12I-PL-2 (ARIAD Gene Therapeutics Inc, Cambridge, MA, USA). The resulting plasmid was named pZ12-EGFP. To prepare pSV40-Hyg, pGL4.16 (Promega, Madison, WI, USA) was digested with BamHI and BglII followed by religation of the resulting larger fragment.

2.2. Cell culture, transfection, and isolation of cell lines

C3H/10T1/2-fLuc and C3H/10T1/2-VEGF cells, derived from C3H/10T1/2 cells (ATCC CCL-226) as described elsewhere [13], stably incorporate a heat-activated and dimerizer-dependent gene switch that controls a firefly luciferase (*fluc)* gene or a human vascular endothelial growth factor isoform 165 (*VEGF165*) gene, respectively. Transfection of HeLa cells (ATCC CCL-2) was carried out using Lipofectamine 2000 (Invitrogen, Barcelona, Spain) following the manufacturer's recommendations. HeLa cells stably harboring the Hsp70/12xZFHD1-TA transactivator construct [13] were isolated using 600 μg mL^{-1} G418 (InvivoGen, San Diego, CA, USA). Stable clones were screened for heat and rapamycin responsiveness after transient transfection with pZ12-fLuc [13]. One day after lipofection, cells were treated for 1 h with rapamycin (Invivogen) or vehicle and then subjected or not to heat treatment at 45°C for 30 min in a thermostatically-controlled water bath. A highly inducible clone was isolated and then cotransfected with pZ12-EGFP and pSV40-Hyg at a 5:1 molar ratio. Clones were isolated subsequent to selection using 600 μg mL^{-1} G418 and 200 μg/mL hygromycin B (InvivoGen). For EGFP induction assays, cells were seeded in 24-wells plates (Sigma-Aldrich, Madrid, Spain) at a density of 2.5×10^4 cells cm^{-2}. One day later, cells were or were not subjected to heat treatment in the presence of rapamycin or vehicle and then cultured further for 24 h. Cells were visualized using a fluorescence microscope Leica AF6000 (Leica Microsystems, Heidelberg, Germany). The average fluorescence of 10 individual fields for each condition was measured using Fiji, an open source image processing package based on ImageJ (http://fiji.sc). A cell line, termed HeLa-EGFP, was identified that exhibited strong transgene expression exclusively after heat treatment in the presence of rapamycin. Clonal C3H/10T1/2- and HeLa-derived cells were

maintained in a humidified 5% CO_2 atmosphere at 37°C in Dulbecco's modified Eagle's medium (DMEM; Lonza, Madrid, Spain) supplemented with 10% (v/v) fetal bovine serum (FBS), 100 U mL^{-1} penicillin and 0.1 mg mL^{-1} streptomycin, under continuous selection with G418 and hygromycin B.

2.3. Rapamycin

For *in vitro* experiments, rapamycin was dissolved in DMSO and used at a final concentration of 10 nM. For *in vivo* injections, rapamycin was dissolved in N, N-dimethylacetamide (DMA) to prepare a stock solution (3 mg mL^{-1}) which was then diluted in a mixture of 50% DMA, 45% polyoxythylene glycol (average molecular weight of 400 Da) and 5% polyoxyethylene sorbitan monooleate (both from Sigma-Aldrich). Rapamycin was injected intraperitoneally at a dose of 1 mg kg^{-1} in a volume of 50 μL.

2.4. Preparation of fibrin-based plasmonic hydrogels

To prepare plasmonic scaffolds, bovine fibrinogen (fbg; Sigma-Aldrich) was dissolved in ice-cold DMEM at a concentration of 20 mg mL^{-1} of clottable protein. HGNPs, synthetized as described elsewhere [10], were added to the fbg solution at 0.02-0.1 mg mL^{-1}. Next, 0.8 volumes of DMEM alone or DMEM containing C3H/10T1/2-fLuc, C3H/10T1/2-VEGF or HeLa-EGFP cells at 2.5×10^6 mL^{-1} were added to the mixture. Finally, 0.2 volumes of ice-cold 20 U mL^{-1} bovine thrombin (Sigma-Aldrich) in DMEM were added. After pipetting briefly to ensure uniform dispersion of components, the suspension was distributed to multiwell culture plates or polystyrene cuvettes (all from Sigma-Aldrich). Final volumes of suspensions were 0.5, 1 or 2 mL for 48-, 24- or 12-well plates, respectively, and 3 mL for polystyrene cuvettes. Suspensions were allowed to clot in a humidified 5% CO_2 atmosphere at 37°C for 30 min. After clotting, 1 volume of DMEM containing 20% FBS was incubated with the hydrogel for 1 h to equilibrate its serum content and then replaced with culture medium. In some experiments the suspensions were supplemented with 30 μg mL^{-1} fbg-Alexa Fluor 546 (fbg-AF546, Invitrogen). To determine cell-mediated biodegradation of scaffolds, release of fbg-AF546 into culture medium was measured after excitation at 558 nm and quantification of the emitted fluorescence at 573 nm, using a Synergy4 spectrofluorimeter (BioTek Instruments, Vermont, USA).

2.5. Rheology

Small deformation oscillatory measurements were carried out in an AR-G2 controlled stress rheometer (TA Instruments, New Castle, DE, USA). The linear viscoelastic region (LVR) was determined through stress sweeps performed at 37°C and an oscillatory frequency of 1 Hz. Frequency sweeps were performed at 37°C between 0.1 and 100 Hz and an oscillatory strain of 0.5% within the LVR. Finally, temperature sweeps between 10 and 80°C were recorded at an oscillatory frequency of 1 Hz and an oscillatory strain of 0.5%.

2.6. Electron microscopy

Scanning transmission electron microscopy (STEM) images of HGNPs were obtained with a Tecnai T30 electron microscope (FEI, Hillsboro, OR, USA) operated in the bright field mode at an accelerating voltage of 300 kV. To characterize plasmonic matrices using

transmission electron microscopy (TEM), the above-described components for preparing plasmonic scaffolds were mixed and then diluted ten-fold in phosphate-buffered saline (PBS). A drop of this dilution was carefully placed on a 400-mesh carbon-coated copper grid and allowed to polymerize for 5 min at 37°C. After removing the excess solution with a filter paper, the sample was visualized using a JEM 1010 electron microscope (JEOL, Peabody, MA, USA). The internal morphology of plasmonic scaffolds, lacking or containing cells, was visualized by scanning electron microscopy (SEM). Hydrogels were rinsed gently with PBS, fixed with 4% paraformaldehyde (PFA) and sliced using a scalpel blade. Slices were lyophilized at -80°C and then mounted on aluminium stubs, sputter-coated with carbon and imaged with a FEI Quanta 200 electron microscope.

2.7. Cell viability assays

Viability of cells entrapped in hydrogels was investigated using the alamarBlue-based assay (Biosource, Nivelles, Belgium). After washing with PBS, samples were incubated in DMEM-10% FBS containing 10% (v/v) alamarBlue dye for 2 h at 37°C. After excitation at 530 nm, emitted fluorescence at 590 nm was quantified using a Synergy4 spectrofluorimeter. Cell viability was additionally assessed by staining with 50 μM calcein violet-acetomethyl ester (Calcein violet AM, Invitrogen). Samples were cultured in the presence of the dye for 2 h and then rinsed gently with PBS and fixed with 10% PFA. After laser excitation at 400 nm, emitted fluorescence at 452 nm was analyzed by biomapping as described below.

2.8. NIR irradiation of fibrin-based hydrogels

The NIR irradiation set-up consisted of an 808 nm laser module with 400 μm fiber coupling (MXL-III(FC) model, Changchun New Industries Optoelectronics Technology Co., Ltd., Changchun, China) connected to a fixed focus collimator (Thorlabs, Newton, NJ, USA) and a silicon photodiode sensor (Model PD300-3W, Ophir Laser Measurement Group, Logan, UT, USA). The fiber optic was coupled to a micropositioning system. For *in vitro* assays, the fiber optic and the positioning system were placed in a thermostatically-controlled chamber (Model Stuart SI60D, Fisher Scientific Afora, Madrid, Spain) to establish the environmental temperature at 37°C. Temperature changes in the hydrogels were monitored by IR thermography using a Testo 875-2i thermal imaging camera (Instrumentos Testo S.A, Madrid, Spain).

2.9. Animal experiments

All procedures were approved by the Animal Welfare Committee of La Paz University Hospital-IdiPAZ and were in compliance with Spanish and European legislation. For subcutaneous implants, components of fibrin hydrogels were mixed as described above with C3H/10T1/2-fLuc or C3H/10T1/2-VEGF cells at a final concentration of 2×10^6 cells mL^{-1}, in a final volume of 500 or 750 μL for fLuc activity or human VEGF secretion assays, respectively. The suspensions were injected subcutaneously into the backs of 4-5 weeks old C3H/HeNRj mice (Janvier-Labs, St Berthevin Cedex, France). Prior to injection, hair was removed from implantation areas by shaving and depilatory treatment, and animals were anesthetized with isoflurane (5% for induction and 2% for maintenance; Baxter, Madrid,

Spain). During implant polymerization *in situ*, mice were kept stationary for 5 min and subsequently placed in the recovery cage. After 24 h, rapamycin was administered. Ninety min later mice were anesthetized, and implant areas were NIR-irradiated. Temperature changes in the body surface were monitored by IR thermography as above-described. Skin overlying implants was photographed and erythematous areas were measured using Fiji software. Animals were euthanized and implants, including surrounding skin and muscle layers, were surgically removed.

2.10. Measurement of target gene activity

EGFP in hydrogels was visualized by biomapping using a confocal laser scanning microscope (Leica TCS-SP5 AOBS, Leica). An 8×8 square of 1.55×1.55 mm Z-stacks covering the hydrogel was acquired with a 10×0.5 N.A dry objective and the confocal images were analyzed using Leica software LAS AF, version 2.6.0.7266. After image reconstruction, areas containing EGFP expressing cells were manually outlined from projected views, and their sizes measured using Fiji software. For human *VEGF165* transgene induction assays, VEGF secretion was measured using a commercially available ELISA kit (R&D Systems, Inc., Minneapolis, MN, USA). For *in vitro* bioluminescence imaging assays, D-luciferin (Promega) was added to culture medium at a final concentration of 80 μg mL^{-1} and 30 min later, the luminescence signal was captured on an IVIS charge-coupled device camera system (PerkinElmer, Waltham, MA, USA). For *in vivo* bioluminescence imaging, mice were anesthetized with isoflurane, and 50 μL of a solution of 40 mg mL^{-1} D-luciferin in PBS were injected subcutaneously near the implant region. Immediately afterwards, animals were imaged using the bioluminescence device described above. Light acquisition was analyzed using the Living Image 4.0 software (PerkinElmer).

2.11. Histology

Formalin-fixed samples were dehydrated through a series of graded ethanols, xylol, and finally xylene, and were embedded in paraffin. Five-micrometer sections were deparaffinized, rehydrated and stained with hematoxylin and eosin (Sigma-Aldrich). Images of the sections were captured using an Olympus BX41 microscope (Olympus, Tokyo, Japan).

2.12. Statistics

Statistical analysis was performed by ANOVA and Turkey's post-hoc tests. Experimental data are reported as means and ± standard deviation (SD). $p<0.05$ was established as the level of statistical significance.

3. Results

3.1. Characterization of fibrin-based plasmonic hydrogels

Fig. 1a displays a representative STEM micrograph of HGNPs. These plasmonic nanostructures, with an average diameter of ~36 nm and a thickness of ~8 nm, were incorporated in fibrin hydrogels (Fig. 1b, left). SEM observation of fibrin-based plasmonic hydrogels revealed a 3-dimensional highly porous structure (Fig. 1b, center). TEM imaging of the protein matrix showed that HGNPs attach to fibrin fibers (Fig. 1b, right), likely due to

entrapment of the nanostructures within the protein mesh during polymerization. Fig. 1c shows that the inclusion of HGNPs in the hydrogels significantly modifies their viscoelastic properties. Storage modulus (G') values increase with HGNPs content. On the other hand, the critical stress point at which stress-softening is observed acquires a higher value with increasing concentration of HGNPs (Fig. 1c, left and center graph). This behavior corresponds to a reinforcing effect of the fibrils as a greater amount of HGNPs are incorporated into hydrogel composition. A study of the influence of temperature on the viscoelastic properties of plasmonic gels revealed that G' values reach a pseudo-equilibrium plateau at temperatures below 30°C (Fig. 1c, right graph). A rheological transition occurs at ~44°C and the elastic modulus experiences a decrease that proved to be reversible in additional experiments (not shown). Finally, another transition takes place at ~73°C and the elastic modulus increases with temperature irreversibly. HGNPs content does not influence transition temperatures.

For solid gold nanospheres about 50 nm in diameter, the peak of surface plasmon absorption is positioned at about 520 nm. By using hollow instead of solid gold spheres and adjusting wall thickness and particle size it is possible to achieve peak plasmon absorption at a desired wavelength within much of the visible and the infrared spectral ranges. The HGNPs used in the present work show a LSPR peak positioned at ~750 nm (Fig.1a, inset). Ultraviolet-visible spectroscopy revealed that upon incorporation of HGNPs, hydrogels gain the ability to efficiently absorb NIR light ("HGNPs +" in Fig. 1d). IR-thermal imaging of hydrogels irradiated with an 808 nm laser diode (see the experimental setting in Fig. 1e) showed a rapid temperature increase in HGNPs-containing matrices (Fig. 1f). Temperature in the hydrogels increased as a function of the amount of HGNPs embedded in the fibrin network. As can be observed in the thermograms, the laser heats the hydrogel through the culture medium that is essentially transparent to 808 nm radiation. At elevated temperatures, the heated hydrogel appears to give rise to convection currents that progressively heat the culture medium. In the absence of HGNPs, irradiation only marginally increases the temperature of the hydrogel (~2.8 °C at the hottest point after 10 min of laser exposure), likely due to scattering and marginal absorption of the incident light passing through the protein matrix.

3.2. Patterning in vitro transgene expression by NIR irradiation of plasmonic hydrogels

HeLa- or C3H/10T1/2-derived cells entrapped in HGNPs-doped hydrogels were imaged by SEM (Fig. 2a). Despite differences in their morphologic characteristics, both cell types distribute homogeneously within hydrogels and secreted an extracellular matrix layer intimately adhered to the scaffold surface. Metabolic activities of HeLa-EGFP or C3H/10T1/2-fLuc cells increased by about two fold after 4 or 6 days of culture, respectively, indicating that cells are able to proliferate within these hydrogels (Fig. 2b). The fibrinolytic activity of C3H/10T1/2-fLuc cells was not affected by HGNPs, suggesting that the cellular ability for remodeling the scaffold is well preserved (Fig. 2c). Collectively, these results indicate that plasmonic hydrogels are suitable scaffolds for supporting cell survival.

To test whether induced optical hyperthermia may be finely tuned to trigger transgene expression, we used HeLa-EGFP cells that stably harbor an *egfp* reporter gene under the

control of the heat-activated and dimerizer-dependent gene expression system outlined in Fig. S1a. In these cells, levels of EGFP expression increase as a function of the intensity of the activating heat treatment (Fig. S1b). Only when heating conditions are too harsh (e.g. exposure at 45°C for 60 min), the fluorescence intensity decreases, owing to cell damage caused by the treatment. HeLa-EGFP cells were encapsulated in fibrin matrices comprising 0.03 mg mL^{-1} HGNPs. The resulting hydrogels were exposed to NIR irradiation at 44 mW mm^{-2} for 5 to 20 min in the presence of rapamycin, which induced substantial transgene expression in encapsulated cells (Fig. 2d). EGFP expression expanded radially with the time of irradiation and could be detected along the laser path. However, long periods of laser exposure led to significant loss of EGFP-expressing cells in the laser incidence area, an effect explained by loss of cell viability caused by lethal heating (Fig. 2e). Figure 2f shows that inducibility of transgene expression upon NIR irradiation can also be modulated by changing amounts of HGNPs within hydrogels which affect heat intensity.

Next, we investigated the extent to which optical properties of plasmonic hydrogels can be used to spatially define transgene expression. C3H/10T1/2-fLuc cells were encapsulated in fibrin hydrogels containing 0.03 mg mL^{-1} HGNPs and treated with rapamycin. The plasmonic constructs were NIR-irradiated in multiple adjacent locations by positioning the laser beam in different XY coordinates. This resulted in a “V”-shaped pattern of transgene expression (Fig. 3a, upper panel). Quantification of fLuc activity at a midsection of the irradiated scaffolds revealed a high degree of symmetry in the patterned motif (Fig. 3a, lower panel). Moreover, both transgene levels as well as induced areas could be modulated by controlling irradiation time (Fig. 3a, right). Finally, cross-sectional views of the irradiated regions revealed that fLuc activity can be detected along the laser-path in the Z axis (Fig. 3b). Collectively, these results show that patterns or gradients of transgene expression can be generated upon NIR irradiation of cell constructs.

3.3. In vivo transgene expression by NIR irradiation of plasmonic hydrogels

To evaluate whether plasmonic matrices are suitable tools for generating localized hyperthermia *in vivo*, we injected subcutaneously hydrogels comprising 0.03-0.05 mg mL^{-1} HGNPs into the backs of adult mice. After 24 h, animals were NIR-irradiated at the implantation site up to 5 min using the experimental setup shown in Fig. 4a. IR thermography showed that body surface temperature in the implanted area increases as a function of HGNPs content in the hydrogel (Fig. 4b). Increasing the power output of the irradiating NIR laser augments the temperature rise at the implantation site. It is worth noting that damage to the host skin was not observed, demonstrating the suitability of the approach as a method for safely inducing mild hyperthermia *in vivo*. Moreover, plasmonic hydrogels could be re-heated by NIR irradiation 4 weeks post-implantation without loss of heating power (Fig. 4c), suggesting that most, if not all, of the plasmonic nanomaterial remained at the implantation site despite hydrogel biodegradation. Interestingly, maximal temperature attained by the hydrogels during heating increased with time in this longitudinal study, although the hydrogels were irradiated with an equivalent dose of NIR energy. This effect may be attributed to progressive shrinkage of the fibrin matrix (not shown), which results in an increased concentration of the metal component.

Next, we investigated whether transgene expression could be triggered *in vivo* in cells comprised in plasmonic hydrogels. C3HT101/2-fLuc cells were injected along with the precursors of fibrin matrices in the subcutaneous space of mice. After 24 h, the animals were treated with rapamycin and NIR-irradiated at the implantation site for 15 min. IR thermograms revealed that irradiation of hydrogels containing HGNPs increased body surface to temperatures between 42-45°C (Fig. 5a, insets). One day later, *in vivo* bioluminescence imaging showed that fLuc expression had been triggered exclusively in cells encapsulated within plasmonic hydrogels, whereby the intensity of radiated luminescence was a function of HGNPs content (Fig. 5a). Treatments that induced transgene expression did not generate any significant tissue damage or signs of inflammatory reactions in the host, as shown in the photographs of implanted areas and histological cross sections of skin overlying the implant or muscle from beneath the hydrogel (Fig. 5b). The histological analysis of the skin confirmed the absence of alterations in epidermal or dermal structures of irradiated animals, while no evidences of hemorrhage or vascular destruction were detected in their dermal or subcutaneous layers.

To explore the ability of this technology to deliberately generate transgenic expression patterns *in vivo*, animals were treated with rapamycin and the implanted area was NIR-irradiated at three adjacent locations. Bioluminescence images taken one day after NIR irradiation demonstrated that fLuc expression can be induced in separate regions of a single plasmonic scaffold (Fig. 5c, left panel). fLuc activity gradually decayed thereafter and could not be detected 6 days post-activation (not shown). When the mice were re-administered rapamycin and the previously irradiated hydrogels were subjected to a second round of NIR irradiation, transgene expression in the hydrogels was re-induced, showing a spatial pattern that matched the NIR-illuminated areas (Fig. 5c, right panel).

3.4. Remote induction of VEGF release by NIR irradiation of plasmonic hydrogels

A final series of experiments examined whether secretion of a transgenic growth factor could be controlled locally using the optical properties of plasmonic hydrogels. To perform this study we encapsulated C3H/10T1/2-VEGF cells in fibrin scaffolds that did or did not contain HGNPs. One day after NIR irradiation at 44 mW mm^{-2} in the presence of rapamycin, we measured the secretion of VEGF in the culture medium. Compared to hydrogels lacking the plasmonic component, irradiation of HGNPs-containing scaffolds for 5 or 10 min resulted in a 130- or 275- fold increase, respectively, of VEGF levels in the culture medium (Fig. 6a). Next, C3H/10T1/2-VEGF cells were injected along with the other hydrogel components in the subcutaneous space of mice. After 24 h, animals were treated with rapamycin and irradiated at two discrete locations within implantation region. Well-defined erythemas were visible four days after NIR irradiation in the skin overlying the hydrogel at laser-illuminated locations (Fig. 6b). These hyperemic regions were confined to within the irradiated area, i.e. the VEGF response could be spatially defined by controlling the irradiation pattern. Induced erythemas had an average size of 3.4 ± 0.9 % of the total implant surface area and could not be detected in animals bearing hydrogels devoid of HGNPs (Fig. 6b).

4. Discussion

The goal of this study was to evaluate the ability of plasmonic scaffolds to function as transducers that convert light into heat at wavelengths within the so called “tissue optical window”, as well as their usefulness in remote patterning of transgene expression. Towards this end, we used fibrin-HGNPs composites to entrap cells harboring a transgene of interest activated by low heat in the presence of a low molecular weight ligand.

Fibrinogen- and fibrin-based scaffolds provide biomimetic environments for cellular attachment, proliferation, migration, differentiation and morphogenesis that support the regeneration of connective tissues, such as skin, ligaments, tendons, blood vessels, cartilage and bone [14-18]. We demonstrated that incorporation of HGNPs during thrombin-induced gelation of fibrinogen resulted in the inclusion of the nanomaterial within the final fibrin hydrogel assembly. The presence of the HGNPs enhanced the mechanical stiffness of the hydrogel as well as enabled it to rapidly convert incident NIR light into heat. Cell survival within the fibrin matrix was not significantly impaired after incorporation of HGNPs, showing that major healing advantages of fibrin scaffolds in tissue engineering applications based on cell-matrix and cell-cell interactions [19] are not affected by the incorporation of HGNPs in their structures. Rapid and complete integration into the host tissue are key factors for the clinical success of scaffolds. Fibrin hydrogels offer the advantage of complete degradation by the fibrinolytic system governed by the protease plasmin [20]. Most fibrin preparations contain the zymogen plasminogen which is cleaved by tissue- or urokinase-type plasminogen activators produced by cells to yield the active form of plasmin [21,22]. Plasmonic fibrin scaffolds retain the ability to be degraded and remodeled by C3H/T101/2-derived cells. In experiments which followed the progress of implanted hydrogels for nearly a month, we observed that shrinkage of composites occurred at a same rate as matrices free of the metal component, dispelling concerns relating to a potential inhibition of the natural fibrinolysis process that could limit scaffold remodeling into tissue. For those tissue engineering applications where optimal shape integrity and stability of the scaffold are required for defined periods of time, HGNPs may be incorporated in hydrogel formulations designed to prolong the life of fibrin matrices, containing, for example, proteolytic or fibrinolytic inhibitors [23-26], cross-linking enzymes such as the transglutaminasa factor XIIIa [27] or reinforcing synthetic polymers such as polyethylene glycol [28] or polyurethane [29]. A remaining issue concerns the toxicity of HGNPs. It is generally assumed that GNPs of sizes > 5 nm are chemically inert like the bulk material and show good biocompatibility [30-32]. Recent reports indicate that, in addition to size, many other factors such as shape, functionalization, doses or administration routes may affect the biodistribution and toxicity of nanoparticulated gold [33-35]. For photothermal ablation therapy, Maltzahn et al.[36] used a dose of 20 mg kg^{-1} of gold nanorods injected intravenously and did not observe any toxicity in tumor-bearing or tumor-free mice. The same dose of PEG-coated hollow gold nanospheres administered intravenously to mice was not toxic, although substantial accumulation of nanomaterial was detected in liver and correlated with irreversible changes in the proteomic profile of this organ [37]. Our approach likely involves gradual release of relatively low doses of nanometal into surrounding host tissues which did not cause discernible local damage. Future studies will

address the possible toxicological or immunological consequences of long-term bioaccumulation of HGNPs in the mononuclear phagocyte system and will explore the use of NIR resonant nanomaterials with improved biodegradability profiles [37].

Photothermal treatments driven by plasmonic nanomaterials such as carbon nanohorns [9], silica-gold nanoshells or HGNPs [10] have proven useful for local activation of transgenes controlled by thermosensitive promoters. These approaches rely on the transient activation of *HSP* promoters, which are silenced within a period of at most a few hours from the activating heat treatment, thus limiting transgene induction to a very narrow time window that may not be compatible with therapies requiring an effective level of a therapeutic protein over a longer period of time. A more important safety concern relates to the possibility that *HSP* promoter-controlled transgenes can be activated inadvertently by a rise in body temperature caused by disease, strenuous exercise or certain pharmacological interventions [3]. Both problems, i.e., insufficiently long periods of transgene expression and the possibility of involuntary promoter activation, were avoided by synthetic regulatory circuits that combine an *HSP70B* promoter and a small molecule-dependent transactivator [38]. In this work, we used a gene switch based on a dimerizer-dependent transactivator whose levels are replenished by a feedforward loop that, in the presence of dimerizer, sustains activated transgene expression for about 8 days after heat activation [13]. Ongoing work is exploring whether heat-activated switches that utilize different ligand-controlled transactivators can be used in combination to regulate the expression profile of multiple transgenes that need to be expressed in a sequential fashion.

The magnitude of transgene induction is dependent on the HGNP concentration in plasmonic fibrin scaffolds as well as on the intensity of the electromagnetic energy delivered to the scaffolds. We determined empirically that a laser power density of 17 mW mm^{-2} applied for 10-15 min triggers robust fLuc expression in plasmonic cell constructs implanted in immunocompetent mice. Miyako et al. [9] used similar output levels of a 785 nm laser to activate the expression of a *fluc* gene driven by a human *HSP70* promoter (*HSPA1A*) in NIH-3T3 cells injected subcutaneously in nude mice along with carbon nanohorns. Exposure to laser irradiation for 30 min increased body surface temperature to 45°C which resulted in visible burn injuries. Likely due to shorter irradiation times, our approach prevented damage to host tissues even when surface temperatures at the implantation site were as high as 44-45°C. An important advantage displayed by the method presented here is the ability to generate desired transgene expression patterns by NIR irradiation of the target regions of choice. This feature is supported by the fairly stable confinement of HGNPs within the matrices, which allows for efficient transduction of photon energy into heat even in long-term implants. In addition to unidentified changes in the physical properties of HGNPs that may occur with time *in vivo*, the observed shrinkage of composites may contribute to a change of their microarchitecture that leads to an increase of the local concentration of trapped nanoparticles. Finally, we demonstrated that the optical properties of plasmonic hydrogels can be efficiently exploited to deliberately control the spatiotemporal bioavailability of an angiogenic growth factor by means of a heat-activated and rapamycin-dependent gene switch. In the presence of the dimerizer, laser treatment of plasmonic hydrogels harboring C3H/T101/2-VEGF cells led to the secretion of large

amounts of VEGF *in vitro*, and to the generation of erythematous wound beds lining the fibrin construct on mice skin. Notably, those external signs of increased vascular permeability and hyperemia were confined to the laser-illumination locations within the implantation area.

In summary, we have shown that NIR irradiation is a suitable tool for deliberately patterning transgene expression in plasmonic cell constructs. This strategy may be useful for achieving spatiotemporal control over the bioavailability of regenerative factors, thus harnessing mechanisms for tissue healing and repair. Being not restricted to specific resonant nanomaterials or scaffold compositions, the combination of remote spatial control by means of NIR laser illumination with safe and timed transgene induction opens a plethora of opportunities for engineering tissues of different developmental origins in regenerative medicine approaches.

5. Conclusions

HGNPs were incorporated to fibrin hydrogels, generating scaffolds responsive to NIR light. Cells harboring a transgene expression system triggered by heat and dependent on a dimerizer-controlled chimeric transactivator were encapsulated in these plasmonic composites. NIR irradiation in combination with dimerizer administration induced *in vitro* and *in vivo* transgene expression with spatial patterns that matched the NIR-illuminated region. The magnitude of transgene induction was dependent on the HGNP concentration within the fibrin hydrogel as well as on the intensity of the electromagnetic energy delivered to the plasmonic scaffold and the irradiation time. The spatiotemporal bioavailability of transgenic VEGF could be controlled *in vivo* using this non-invasive technology.

Supplementary Material

Refer to Web version on PubMed Central for supplementary material.

Acknowledgments

The authors are greatly indebted to M. Prieto (Universidad de Zaragoza) for assistance with UV-VIS absorption experiments of plasmonic scaffolds, D. Morales (Confocal Microscopy Laboratory, Universidad Autónoma de Madrid, Spain) for support with the biomapping experiments, F. Urbano, C. Aguado (Transmission Electron Microscopy Service, Universidad Autónoma de Madrid) and L. Tormo (SEM laboratory of the National Museum of Science and Technology of Madrid, Spain) for technical support with TEM and SEM imaging, and I. Martín (Instituto de Investigaciones Biomédicas “Alberto Sols”, Universidad Autónoma de Madrid-CSIC, Spain) for sharing the bioluminescence imaging facility. This work was supported by grants PI12/01698 from Fondo de Investigaciones Sanitarias (FIS, Spanish Ministry of Economy and Competitiveness, MINECO, Spain), MAT2011-24988 and MAT2011-24797 from former Spanish Ministry of Science and Innovation (MICINN), United States Department of Defense Grant OR090134, National Institutes of Health Grant R01 DE013386 and by HSF Pharmaceuticals S.A. F.M.M S. was supported by program Sara Borrell from FIS. C.G.W. was supported by a postdoctoral fellowship through NIH graining grant T32DE007057-34. N.V. is supported by Program I2 from Comunidad de Madrid (Spain).

References

[1]. Zhao X, Kim J, Cezar CA, Huebsch N, Lee K, Bouhadir K, et al. Active scaffolds for on-demand drug and cell delivery. Proc Natl Acad Sci USA. 2011; 108:67–72. [PubMed: 21149682]

[2]. Ziv-Polat O, Skaat H, Shahar A, Margel S. Novel magnetic fibrin hydrogel scaffolds containing thrombin and growth factors conjugated iron oxide nanoparticles for tissue engineering. Int. J. Nanomedicine. 2012; 7:1259–74. [PubMed: 22419873]

[3]. Vilaboa N, Voellmy R. Regulatable gene expression systems for gene therapy. Curr Gene Ther. 2006; 6:421–38. [PubMed: 16918333]

[4]. Wang X, Chen X, Yang Y. Spatiotemporal control of gene expression by a light-switchable transgene system. Nat Methods. 2012; 9:266–9. [PubMed: 22327833]

[5]. Dreano M, Brochot J, Myers A, Cheng-Meyer C, Rungger D, Voellmy R, et al. High-level, heat-regulated synthesis of proteins in eukaryotic cells. Gene. 1986; 49:1–8. [PubMed: 3569912]

[6]. Deckers R, Quesson B, Arsaut J, Eimer S, Couillaud F, Moonen CT. Image-guided, noninvasive, spatiotemporal control of gene expression. Proc Natl Acad Sci USA. 2009; 106:1175–80. [PubMed: 19164593]

[7]. Wilson CG, Martin-Saavedra FM, Padilla F, Fabiilli ML, Zhang M, Baez AM, et al. Patterning expression of regenerative growth factors using high intensity focused ultrasound. Tissue Eng, Part C. 2014 in press.

[8]. Laughner JL, Sulkin MS, Wu Z, Deng CX, Efimov IR. Three potential mechanisms for failure of HIFU ablation in cardiac tissue. Circ Arrhythm Electrophysiol. 2012; 5:409–16. [PubMed: 22322367]

[9]. Miyako E, Deguchi T, Nakajima Y, Yudasaka M, Hagihara Y, Horie M, et al. Photothermic regulation of gene expression triggered by laser-induced carbon nanohorns. Proc Natl Acad Sci USA. 2012; 109:7523–8. [PubMed: 22529368]

[10]. Cebrian V, Martin-Saavedra F, Gomez L, Arruebo M, Santamaria J, Vilaboa N. Enhancing of plasmonic photothermal therapy through heat-inducible transgene activity. Nanomedicine (NY, NY, US). 2013; 9:646–56.

[11]. Frangioni JV. In vivo near-infrared fluorescence imaging. Curr Opin Chem Bio. 2003; 7:626–34. [PubMed: 14580568]

[12]. Weissleder R. A clearer vision for in vivo imaging. Nature Biotechnol. 2001; 19:316–7. [PubMed: 11283581]

[13]. Martin-Saavedra FM, Wilson CG, Voellmy R, Vilaboa N, Franceschi RT. Spatiotemporal control of vascular endothelial growth factor expression using a heat-shock-activated, rapamycin-dependent gene switch. Hum. Gene Ther Methods. 2013; 24:160–70. [PubMed: 23527589]

[14]. Gorodetsky R, Vexler A, Levdansky L, Marx G. Fibrin microbeads (FMB) as biodegradable carriers for culturing cells and for accelerating wound healing. J Invest Dermatol. 1999; 112:866–72. [PubMed: 10383731]

[15]. Kalbermatten DF, Kingham PJ, Mahay D, Mantovani C, Petterson J, Raffoul W, et al. Fibrin matrix for suspension of regenerative cells in an artificial nerve conduit. J Plast Reconstr Aesthet Surg. 2008; 61:669–75. [PubMed: 18218346]

[16]. Meinhart J, Fussenegger M, Hobling W. Stabilization of fibrin-chondrocyte constructs for cartilage reconstruction. Ann of Plast Sur. 1999; 42:673–8.

[17]. Park KH, Kim H, Moon S, Na K. Bone morphogenic protein-2 (BMP-2) loaded nanoparticles mixed with human mesenchymal stem cell in fibrin hydrogel for bone tissue engineering. J Biosci Bioeng. 2009; 108:530–7. [PubMed: 19914589]

[18]. Sahni A, Francis CW. Vascular endothelial growth factor binds to fibrinogen and fibrin and stimulates endothelial cell proliferation. Blood. 2000; 96:3772–8. [PubMed: 11090059]

[19]. Janmey PA, Winer JP, Weisel JW. Fibrin gels and their clinical and bioengineering applications. J R Soc Interface. 2009; 6:1–10. [PubMed: 18801715]

[20]. Weisel JW. Fibrinogen and fibrin. Adv Protein Chem. 2005; 70:247–99. [PubMed: 15837518]

[21]. Buchta C, Hedrich HC, Macher M, Hocker P, Redl H. Biochemical characterization of autologous fibrin sealants produced by CryoSeal and Vivostat in comparison to the homologous fibrin sealant product Tissucol/Tisseel. Biomaterials. 2005; 26:6233–41. [PubMed: 15921738]

[22]. Cesarman-Maus G, Hajjar KA. Molecular mechanisms of fibrinolysis. Br J Haematol. 2005; 129:307–21. [PubMed: 15842654]

[23]. Ahmed TA, Griffith M, Hincke M. Characterization and inhibition of fibrin hydrogel-degrading enzymes during development of tissue engineering scaffolds. Tissue Eng. 2007; 13:1469–77. [PubMed: 17518706]

[24]. Kupcsik L, Alini M, Stoddart MJ. Epsilon-aminocaproic acid is a useful fibrin degradation inhibitor for cartilage tissue engineering. Tissue Eng, Part A. 2009; 15:2309–13. [PubMed: 19086806]

[25]. Sperzel M, Huetter J. Evaluation of aprotinin and tranexamic acid in different in vitro and in vivo models of fibrinolysis, coagulation and thrombus formation. J Thromb Haemost. 2007; 5:2113–8. [PubMed: 17666018]

[26]. Lorentz KM, Kontos S, Frey P, Hubbell JA. Engineered aprotinin for improved stability of fibrin biomaterials. Biomaterials. 2011; 32:430–8. [PubMed: 20864171]

[27]. Ariëns RA, Lai TS, Weisel JW, Greenberg CS, Grant PJ. Role of factor XIII in fibrin clot formation and effects of genetic polymorphisms. Blood. 2002; 100:743–54. [PubMed: 12130481]

[28]. Barker TH, Fuller GM, Klinger MM, Feldman DS, Hagood JS. Modification of fibrinogen with poly(ethylene glycol) and its effects on fibrin clot characteristics. J Biomed Mater Res. 2001; 56:529–35. [PubMed: 11400130]

[29]. Wittmann K, Storck K, Muhr C, Mayer H, Regn S, Staudenmaier R, et al. Development of volume-stable adipose tissue constructs using polycaprolactone-based polyurethane scaffolds and fibrin hydrogels. J Tissue Eng Regen Med. 2013 doi:10.1002/term.1830.

[30]. Pan Y, Neuss S, Leifert A, Fischler M, Wen F, Simon U, et al. Size-dependent cytotoxicity of gold nanoparticles. Small. 2007; 3:1941–9. [PubMed: 17963284]

[31]. Yen HJ, Hsu SH, Tsai CL. Cytotoxicity and immunological response of gold and silver nanoparticles of different sizes. Small. 2009; 5:1553–61. [PubMed: 19326357]

[32]. Connor EE, Mwamuka J, Gole A, Murphy CJ, Wyatt MD. Gold nanoparticles are taken up by human cells but do not cause acute cytotoxicity. Small. 2005; 1:325–7. [PubMed: 17193451]

[33]. Alkilany AM, Murphy CJ. Toxicity and cellular uptake of gold nanoparticles: what we have learned so far? J Nanopart Res. 2010; 12:2313–33. [PubMed: 21170131]

[34]. Dykman L, Khlebtsov N. Gold nanoparticles in biomedical applications: recent advances and perspectives. Chem Soc Rev. 2012; 41:2256–82. [PubMed: 22130549]

[35]. Almeida JP, Chen AL, Foster A, Drezek R. In vivo biodistribution of nanoparticles. Nanomedicine (London, UK). 2011; 6:815–35.

[36]. von Maltzahn G, Park JH, Agrawal A, Bandaru NK, Das SK, Sailor MJ, et al. Computationally guided photothermal tumor therapy using long-circulating gold nanorod antennas. Cancer Res. 2009; 69:3892–900. [PubMed: 19366797]

[37]. Guo L, Panderi I, Yan DD, Szulak K, Li Y, Chen YT, et al. A comparative study of hollow copper sulfide nanoparticles and hollow gold nanospheres on degradability and toxicity. ACS Nano. 2013; 7:8780–93. [PubMed: 24053214]

[38]. Vilaboa N, Fenna M, Munson J, Roberts SM, Voellmy R. Novel gene switches for targeted and timed expression of proteins of interest. Mol Ther. 2005; 12:290–8. [PubMed: 15925546]

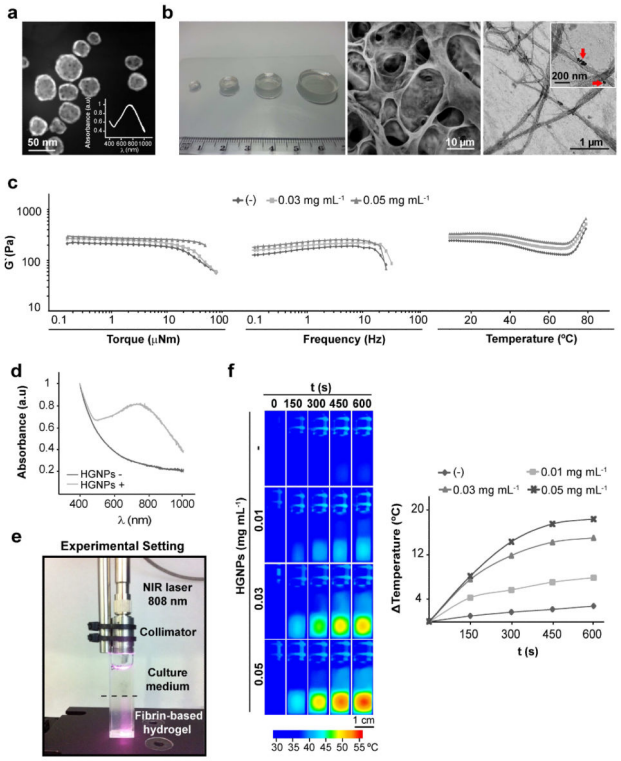

Fig. 1.

Characterization of fibrin-based plasmonic hydrogels. (a) STEM image of HGNPs. Inset shows the absorption spectrum of HGNPs in DMEM. (b) Photograph (left), SEM (center) and TEM (right) images of hydrogels containing 0.03 mg mL^{-1} HGNPs. Arrows in boxed area point to HGNPs encapsulated within fibrin fibers. (c) Dynamical mechanical analysis of hydrogels containing the indicated doses of HGNPs as a function of torque, frequency and temperature. (d) Absorption spectra of fibrin-based hydrogels. (e) Experimental set-up for NIR irradiation of hydrogels. (f) Fibrin hydrogels containing the indicated doses of HGNPs were irradiated with NIR laser at 44 mW mm^{-2} for the indicated times and monitored by IR thermography (left). The graph shows the maximum temperature rise detected during NIR irradiation (right).

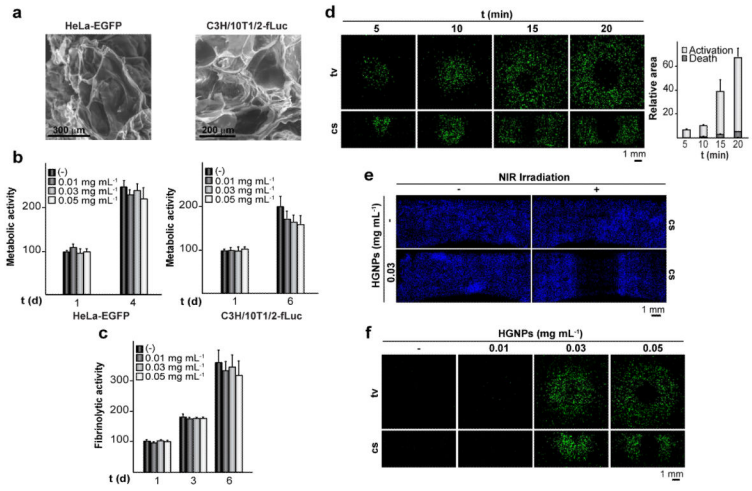

Fig. 2.

Characterization of plasmonic hydrogels as cellular scaffolds. (a) SEM images show HeLa-EGFP or C3H/10T1/2-fLuc cells cultured for 1 day within hydrogels containing 0.03 mg mL^{-1} HGNPs. (b) Graphs show metabolic activities of cells encapsulated within hydrogels containing different doses of HGNPs, at the indicated times of culture. (c) Release of fbg-AF546 to the medium in cultures of C3H/10T1/2-fLuc cells entrapped in hydrogels containing the indicated doses of HGNPs. The data are expressed as the percentage of the fluorescence measured in the media from hydrogels lacking HGNPs cultured for 1 day, which was given the arbitrary value of 100 (b and c). Each value represents the mean ± SD. HeLa-EGFP cells were encapsulated within hydrogels containing 0.03 mg mL^{-1} HGNPs (d and e) or the indicated doses of HGNPs (f) and cultured for 24 h. Constructs were treated with rapamycin and exposed (+) or not (−) to NIR irradiation at 44 mW mm^{-2} for 5-20 min (d), 20 min (e) or 10 min (f), and cultured further for 24 h. Biomappings of top-view (tv) or cross section (cs) of hydrogels show calcein-violet stained cells in blue (e) or EGFP-expressing cells in green (d and f). Graph shows the relative area concentric to the spot of laser incidence comprising cells that express (Activation) or do not express (Death) EGFP in tv images. Values are relative to the total surface area of the hydrogel, which was given the arbitrary value of 100.

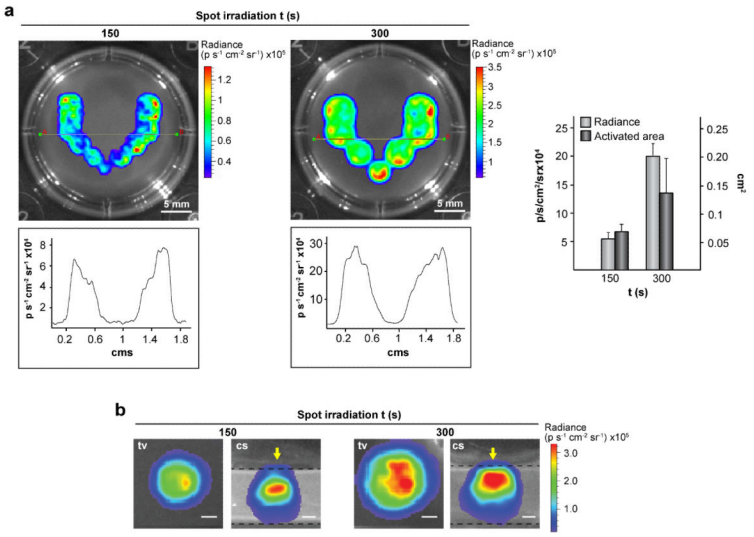

Fig. 3.

Patterning transgene expression using optical hyperthermia. C3H/T101/2-fLuc cells were encapsulated within hydrogels containing 0.03 mg mL^{-1} HGNPs and cultured for 24 h. Constructs were treated with rapamycin, NIR-irradiated at 44 mW mm^{-2} at each spot for the indicated times and cultured further for 24 h before bioluminescence imaging. (a) Top view of hydrogels NIR-irradiated at 11 (left) or 7 (right) adjacent spots (upper panel), and quantification of fLuc activity in the construct midline (lower panel). Graph shows the average luminescence radiance levels and the size of activated areas in induced regions. Each value represents the mean ± SD. (b) Top (tv) and cross-section (cs) views of a single spot exposed to NIR irradiation. Arrows in cs views indicate the direction of NIR laser incidence. Dashed lines delimit the edges of the hydrogel. Scale bars = 1 mm.

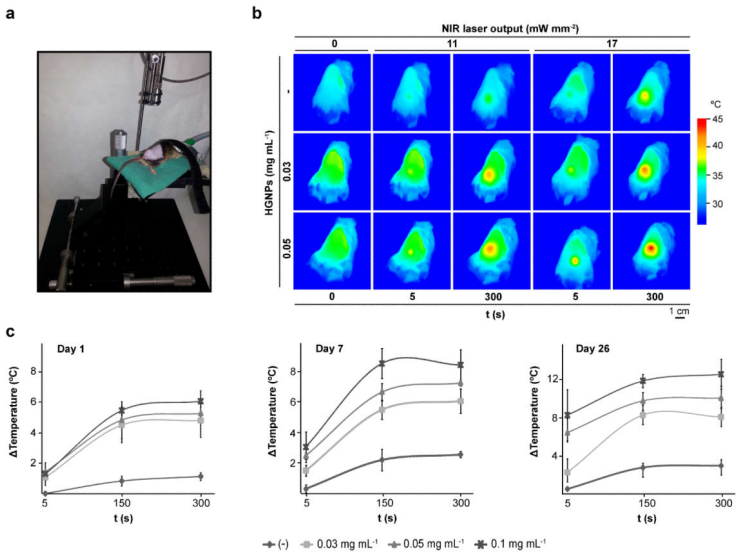

Fig. 4.

In vivo hyperthermia induced by the optical properties of plasmonic hydrogels. (a) Experimental set-up for NIR irradiation of hydrogels *in vivo.* (b) Thermograms of animals implanted with hydrogels containing the indicated doses of HGNPs and NIR-irradiated at a single spot at 11 or 17 mW mm^{-2} for the indicated times. (c) Maximum temperature rise detected at the implantation site during NIR irradiation of same implant at 11 mW mm^{-2} on day 1, 7 and 26 following the implantation. Each value represents the mean ± SD, n = 3.

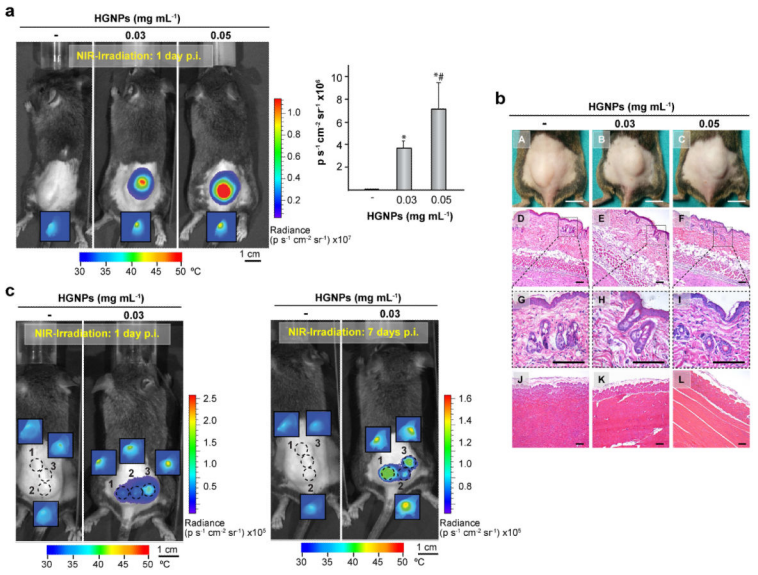

Fig. 5.

In vivo control of *fluc* transgene expression in plasmonic hydrogels. Mice were implanted with hydrogels containing the indicated doses of HGNPs and harboring C3H/10T1/2-fLuc cells. One day after, mice were administered rapamycin and NIR-irradiated at 17 mW mm^{-2} at a single location for 15 min (a) or at three separate locations for 10 min each (c, left panel). Six days later, mice were re-administered rapamycin and subjected to a second irradiation treatment (c, right panel). Bioluminescence imaging was performed 24 h after NIR irradiation. Dashed circles in (c) indicate laser incidence areas. Insets show thermograms of implantation areas at the end of NIR irradiation. Graph shows average luminescence radiance levels detected at the implantation site in (a). *: $p<0.05$ compared to hydrogels lacking HGNPs; $^{\#}$: $p<0.05$ compared to hydrogels containing 0.03 mg mL^{-1} HGNPs; n = 6. (b) Photographs of implantation area (A-C) and histology cross-sections of hydrogels sandwiched by skin (D-I) and gluteal muscle (J-L) 24 h after NIR irradiation for 15 min. Dashed boxes (G-I) show 4x magnified images of epidermis and dermis. Scale bars = 1 cm for photographs and 50 μm for histology captions. p.i.: post-implantation.

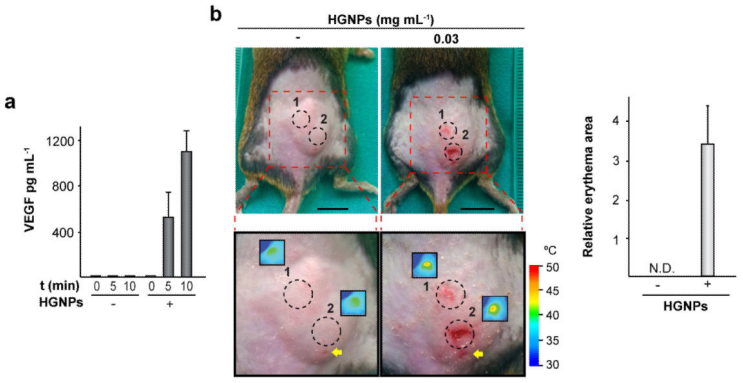

Fig. 6.

Control of human *VEGF165* transgene expression in plasmonic hydrogels. (a) C3H/T101/2-VEGF cells were encapsulated within hydrogels containing (+) or not (−) 0.03 mg mL^{-1} HGNPs and cultured for 24 h. Constructs were treated with rapamycin, exposed to NIR irradiation at 44 mW mm^{-2} for the indicated times and cultured further for 24 h. Media were collected and VEGF secretion was measured. (b) Hydrogels containing the indicated doses of HGNPs and harboring C3H/10T1/2-VEGF cells were NIR-irradiated at 17 mW mm^{-2} at two separate locations for 12.5 min each. Left panel: implantation areas were photographed 4 days after NIR irradiation. Dashed circles in magnified images indicate laser incidence areas. Insets show thermograms of implantation areas after NIR irradiation. Arrows indicate the site of hydrogel injection. Right panel: the graph shows the extent of erythematous skin lesions, relative to the total surface area of the implant. Scale bars = 1 cm. N.D.: not detected.